REPORT DOCUMENTATION PAGE

Form Approved
OMB No. 0704-0188

1. REPORT DATE *(DD-MM-YYYY)*	2. REPORT TYPE	3. DATES COVERED *(From - To)*
20 December 2012	Final Report	July 2010 - May 2012

4. TITLE AND SUBTITLE
Near-Field Acoustic Measurements Using a Line Array in Shallow Water

5a. CONTRACT NUMBER

5b. GRANT NUMBER
N00014-10-1-0935

5c. PROGRAM ELEMENT NUMBER

6. AUTHOR(S)
Dr. D. Christopher Barber, Dr. David L. Bradley

5d. PROJECT NUMBER
18171

5e. TASK NUMBER
01

5f. WORK UNIT NUMBER

7. PERFORMING ORGANIZATION NAME(S) AND ADDRESS(ES)
Applied Research Laboratory
P. O. Box 30
State College, PA 16804-0030

8. PERFORMING ORGANIZATION REPORT NUMBER

9. SPONSORING/MONITORING AGENCY NAME(S) AND ADDRESS(ES)
ONR Reg. Office Chicago-N62880
230 South Dearborn, Room 380
Chicago, IL 60604-1595

10. SPONSOR/MONITOR'S ACRONYM(S)
ONR

11. SPONSOR/MONITOR'S REPORT NUMBER(S)

12. DISTRIBUTION/AVAILABILITY STATEMENT
Approved for public release; distribution is unlimited.

13. SUPPLEMENTARY NOTES

14. ABSTRACT

Results are presented from a test conducted at the US Navy Acoustic Research Detachment in Bayview, Idaho during summers 2010 and 2011. A line of omnidirectional hydrophones was deployed from a barge. A series of test signals was transmitted through calibrated acoustic sources to evaluate the effectiveness of post-processing techniques, as well as line array beamforming, in minimizing reflected path contributions and improving signal-to-noise ratio. A method of estimating the location to the sources while taking into account a real, non linear array based on these measurements are presented.

15. SUBJECT TERMS
hydrophones, acoustics, signal-to-noise ratio, non linear array

16. SECURITY CLASSIFICATION OF:			17. LIMITATION OF ABSTRACT	18. NUMBER OF PAGES	19a. NAME OF RESPONSIBLE PERSON
a. REPORT	b. ABSTRACT	c. THIS PAGE			David L. Bradley for D. Christopher Barber
U	U	U	UU		19b. TELEPHONE NUMBER *(Include area code)* 814-863-7089

Near-Field Beamforming Using a Linear Array in Deep and Shallow Water

David L. Bradley (for D. Christopher Barber)
The Pennsylvania State University/Applied Research Laboratory
State College, PA 16804-0030
(814) 863-7089 e-mail: dlb25@psu.edu

Final report for ONR Grant Number: N00014-10-1-0935
Code 331

Prepared for:
US Office of Naval Research
875 N Randolph Street, Suite 1425
One Liberty Center – Room 272
Code 331
Arlington, VA 22203

ABSTRACT

Noise generated by underwater sources is typically characterized in terms of a far-field, plane-wave equivalent source level based on measurements made in a free-field environment such as a deep water test range. Measurements made in a harbor environment, where multiple reflections, high background noise and short propagation paths are typical, violates these conditions. With careful analysis it may be possible to arrive at a valid estimate of source location and source level from such measurements.

This paper reports results from a test conducted at the US Navy Acoustic Research Detachment in Bayview, Idaho during the summers of 2010 and 2011. A line array of omnidirectional hydrophones was deployed from a barge. A series of test signals was transmitted in both deep and shallow water using calibrated acoustic sources to evaluate the effectiveness of post-processing techniques, as well as line array beamforming, in minimizing reflected path contributions and improving signal-to-noise ratio. A method of estimating the location of the sources while taking into account a real, non linear array based on these measurements is presented.

Table of Contents

List of Figures

LONG-TERM GOALS & OBJECTIVES

Source characterization measurements are best done in a deep water environment where far-field and free-field assumptions can be made. In this case, acoustic waves arriving at the array are approximately planar, and plane wave beamforming can be utilized. This is the only method covered in most array signal processing books. Plane wave beamforming requires that the source is a radiating simple source and the wavefronts received by the array are planar. The far-field is often defined as starting at [1, 2]

$$r = \frac{2L^2}{\lambda} \tag{1}$$

where r is the distance from the center of the array to the source, L is the largest dimension of the array, and λ is the acoustic wavelength. This is the definition that is used throughout this paper.

When the source is closer to the array, wavefront curvature must be taken into consideration. Different methods of accounting for this complexity have been established [1, 2, 3, 4, 5, 6], however few have taken into account the possibility of a curved one-dimensional array and possible error in the location of the array [1, 2, 3], and none have used the near field compensation method of beamforming to account for this. In this paper, a means of source localization is developed which would work in a shallow, multipath environment with the source in the near-field of the array.

APPROACH

This work will present data acquired at the Navy's Acoustics Research Detachment at Lake Pend Oreille in Bayview, Idaho. A 14 element array was deployed in a 45 foot deep water column as well as in deep water (approximately 1200 feet). Two sources were also deployed and a variety of signals were transmitted from each source. The data is processed using the near field compensation method of beamforming assuming a vertical array and compared to results found after using a cross-correlation to determine the actual shape of the array.

The deep water test site is examined first with the array in the far field of the source. This is the simplest situation, and evaluation using delay and sum beamforming in the frequency domain is done to ensure that the algorithm is working properly. This plane-wave beamformer is proven to work well in this free field environment when the array is in the far field of the source. The near field compensation method of beamforming is then used for this case. It is shown that there is little to no difference in the results for both methods. Showing the near field beamformer matches the plane wave beamformer in the far field case proves that the near field beamformer is working properly.

Following these analyses, the deep water test site is once again utilized, but with the array in the near field of the source. This allows for examination of the effect of the array being in the near field without the added complication of multiple reflections. First the plane-wave beamformer is used, and is shown to give inaccurate results. The near field algorithm is then used, giving

accurate results and proving that it works in near field conditions. There is a small error in the location estimate, so a measurement of the array element locations is made to increase accuracy. The algorithm is then adjusted for the different element locations and a new set of results is found that increases accuracy.

Finally, the array and sources are moved into a shallow water, harbor environment. This is a complex environment with many reflections and the array is in the near field of the source. The original near field algorithm is tested as well as the algorithm that has been adjusted for curvature of the array. In the shallow water environment in particular the curvature is very noticeable and making the adjustments for it shows to have increased accuracy.

OBJECTIVES (N/A)

WORK COMPLETED

Multiple methods of beamforming, both far field and near field, are discussed as a background as well as to present methods used in this paper. In the far field regime, standard time delay beamforming is explored in both the time and frequency domains. Two other forms of far field beamforming that are presented in [3] are also discussed, Bartlett beamforming and an adaptive method called the Minimum Variance distortionless processor (MV).

Following these far field approaches, several near field algorithms are discussed. First, the near field compensation method is explored. Following the discussion of this method, Matched Field Processing as presented in [3] is discussed, followed by Radial Reciprocity as presented by Kennedy in [1, 2], Robust Near-Field Adaptive Beamforming as presented by Zheng in [4], and the Chirp Zeta Transform (CZT) as presented by Palmese in [5, 6].

The generic geometry of the test location as well as instrumentation and signals used is presented. More detail on the test site geometry is presented when each different array and source position is discussed later. The array design frequency is also presented.

The processed results of the test data is discussed. Deep water results using a far field conventional beamformer are presented first to establish a baseline. The results using the near field beamforming algorithm is presented next to confirm that it works property. The array is then moved into the source's near field and both conventional beamforming and near field beamforming results are presented. The results of the array element localization calculations are then explored and the method of correction for the error in the vertical array assumption is given. The results of the deep water test using the array curvature modification is then presented. The work then moves into shallow water using the conventional beamforming algorithm, the near field algorithm without accounting for array curvature, and the near field algorithm with the array curvature modification.

Conclusions are drawn. Future work and possibilities are also discussed.

RESULTS

Beamforming is a method of spatial filtering which is analagous to filtering a narrowband signal in the frequency domain. It is used with an array of sensors to accomplish the following goals [7]:

1) Reduce the ambient noise with which a plane wave signal must compete.

2) Permit the separate detection, or resolution, of plane wave signals arriving from different directions.

3) Permit the measurement of the direction of arrival of plane wave signals.

Spatial filtering is compared with frequency domain filtering in Figure 2.1.

Array beamforming is used for source detection, localization, and identification. Many different beamforming methods have been developed over the years.

Far Field Beamforming

Far field beamforming and line array processing are explored in great depth in many textbooks. This paper follows the method shown in Kinsler, Frey, Coppens, and Sanders [8, p. 195]. Consider a line array of hydrophones as shown in Figure 2.2, with N elements and with separation distance d [8]. If a source generates a pressure wave of the form $\left(\frac{A}{r_i'}\right)\exp\left[j\left(\omega t - kr_i'\right)\right]$ that is received by the ith source (where r_i is the distance from the source to the ith element), the averaged pressure received by the array would be:

$$p(r,\theta,t) = \frac{1}{N}\sum_{i=1}^{N}\frac{A}{r_i}e^{j(\omega t - kr_i)} \tag{2.1}$$

Let us define $r_i = r_1 - \frac{1}{2}(i-1)\Delta r$ where $\Delta r = d\sin\theta$. r represents an average distance between the source and the receiver elements. Δr represents the incremental distance between

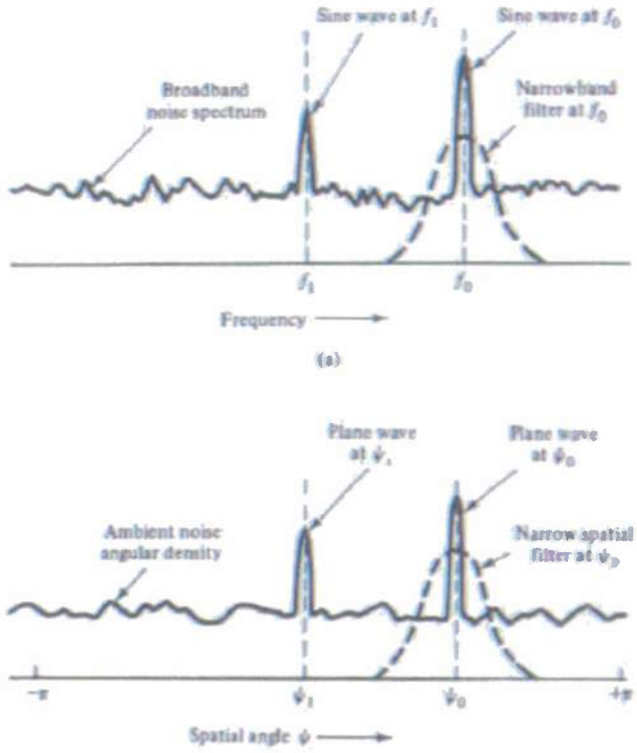

Figure 2.1: Comparison of frequency and spatial domain filter functions: (a) power spectral density of sine-wave signals in broadband noise; (b) angular density of acoustic plane wave signals in ambient noise. (Taken from [7])

receiver elements toward the source. θ is the steering angle.

If the assumption is made that the source is in the far field, where $r \gg (N-1)d$ (where the distance from the array to the source is much larger than the length of the array), then the raypaths between the source and each receiver are relatively parallel. The distance from the source to each element can be defined as $r_i = r_1 - (i-1)\Delta r$, $(i = 1, 2, \ldots, N)$. It is necessary to retain this relationship exactly in the phase, but in the amplitude terms, one may use the far field approximation $\frac{1}{r_i} \approx \frac{1}{r}$. This gives a simplified equation taking these far field assumptions into account:

$$p(r,\theta,t) = \frac{A}{Nr} e^{-j\left(\frac{N-1}{2}\right)k\Delta r} e^{j(\omega t - kr)} \sum_{i=1}^{N} e^{j(i-1)k\Delta r} \tag{2.2}$$

One of the primary forms of beamforming, and the first method presented, is called delay and sum beamforming and it can be done in both the time and frequency domain. The time domain method will be presented first. This method delays each element by a specific time interval based on the difference in path lengths between elements, Δr, which can be calculated from the element

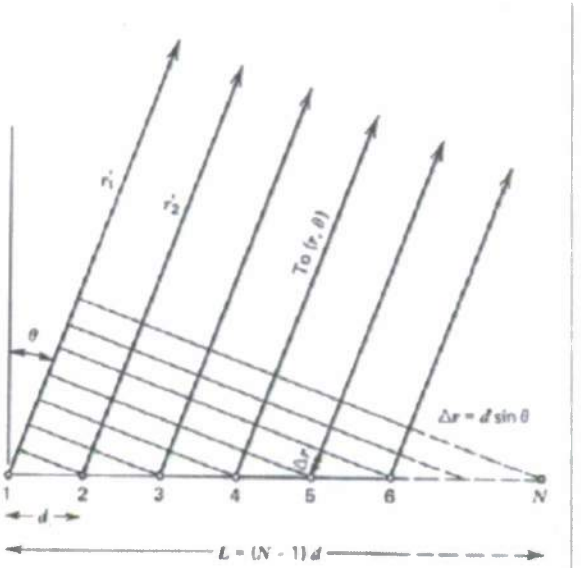

Figure 2.2: Line Array Geometry

separation and the steering angle θ_0:

$$\Delta r = d \sin \theta_0 \tag{2.3}$$

as well as the speed of sound in the medium:

$$\tau = \frac{\Delta r}{c} \tag{2.4}$$

By implementing a time delay and summing over the entire array, the steering angle that receives the most energy can be identified, revealing that to be the angle of incidence and the direction of the source. This also serves to help suppress background noise at angles other than the incident angle. This delay can be added as a phase delay, $e^{j\phi_i}$, where $\phi_i = i\omega\tau = ikd\sin\theta_0$, to Eq. 2.2 to get:

$$p(r, \theta, t, \theta_0) = \frac{A}{Nr} e^{-j\left(\frac{N-1}{2}\right)k\Delta r} e^{j(\omega t - kr)} \sum_{i=1}^{N} e^{j(\phi_i + [i-1]k\Delta r)} \tag{2.5}$$

Delay and sum beamforming can also be performed in the frequency domain. The equation for this can easily be found by performing a Fourier Transform on Eq. 2.5:

$$F(r,\theta,\omega,\theta_0) = \frac{1}{2\pi}\int_{-\frac{T}{2}}^{\frac{T}{2}} \frac{A}{Nr} e^{-j\omega t} e^{j(\omega t - kr)} e^{-j\left(\frac{N-1}{2}\right)k\Delta r} \left(\sum_{i=1}^{N} e^{j(\phi_i + [i-1]k\Delta r)}\right) dt$$

$$= \frac{1}{2\pi}\frac{A}{Nr} e^{-jkr} e^{-j\left(\frac{N-1}{2}\right)k\Delta r} \left(\sum_{i=1}^{N} e^{j(\phi_i + [i-1]k\Delta r)}\right) \int_{-\frac{T}{2}}^{\frac{T}{2}} dt \tag{2.6}$$

This is an unsteered Fast Fourier Transform multiplied by $\sum_{i=1}^{N} e^{j\phi_i}$. In [9], a weighting factor is added to the array to control the sidelobes of the beam pattern.

$$F(k,\theta) = \sum_{i=0}^{N-1} w_i X_i(k) e^{-j(ik\Delta r)} \tag{2.7}$$

where w_n is a weighting coefficient and $X_i(k)$ are the complex-valued coefficients, or our data points. This equation was then vectorized in [10], making the implementation of this method significantly easier and much more computationally manageable:

$$Y(f) = \mathbf{d^H}(\theta, f)\mathbf{W}\mathbf{x}(f) \tag{2.8}$$

Here, θ is the incident angle, $\mathbf{W}$ is a weighting matrix:

$$\mathbf{W} = \text{diag}\{W_1, \ldots, W_n\} \tag{2.9}$$

$\mathbf{d^H}(\theta, f)$ is a steering vector dependent on incident angle, frequency, element spacing, and speed of sound:

$$\mathbf{d^H}(\theta, f) = \left[e^{j2\pi f\Delta r_1} \ldots e^{j2\pi f\Delta r_n}\right]^T \tag{2.10}$$

and $\mathbf{x}(f)$ is the data vector:

$$\mathbf{x}(f) = [X_1(f) \ldots X_n(f)]^T \tag{2.11}$$

Eq. 2.8 can produce a Bearing-Time Record (BTR), which shows where the signal exists in space and time. This can be especially useful in detecting the movement of a source.

Figure 2.3 is a BTR which displays the bearing angle on the x-axis and time on the y-axis. The color axis here displays the sound pressure level in dB re 1 μPa. It can be effectively used to show vertical (or horizontal, depending on the setup of the array) movement of sounds over time. If the source is not moving, a BTR can be collapsed into a more easily readable two-dimensional plot that displays sound pressure level vs. bearing angle. This is shown in Figure 2.4.

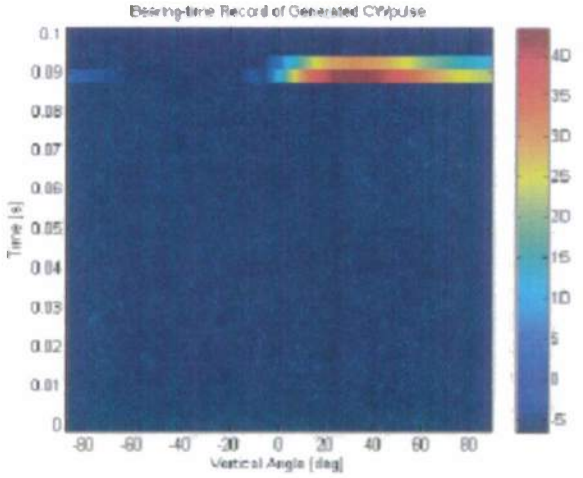

Figure 2.3: Sample Bearing Time Record

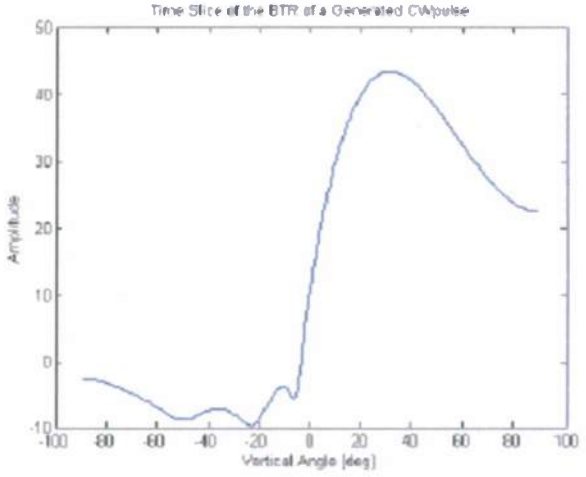

Figure 2.4: Sample Averaged Bearing Time Record

Using these graphs, while the source level can't be known without the range, the angle of incidence can be easily identified.

Bartlett Beamforming

Another very similar algorithm is presented in [3]. This Bartlett beamformer takes the same approach of adding the shaded signal from each hydrophone together to find the incident angle of the signal:

$$B_{Bart}(\theta_s) = \left| \sum_{i=1}^{m} w_i^*(\theta_s)[s_i(\theta) + n_i] \right|^2 = \sum_{i,j=1}^{m} w_i^*(\theta_s)(s_{ij} + n_{ij})w_j(\theta_s) \tag{2.12}$$

Here $s_{ij} + n_{ij}$ are signal and noise that are part of a Cross-Spectral Density Matrix and w_i is the ith element of a steering column vector. Eq. 2.12 can be vectorized using the steering column vector $\mathbf{w}$ and the Cross-Spectral Density Matrix $\mathbf{K}$. The CSDM can be constructed using data vectors $\mathbf{d}$ and using $\dagger$ to represent the complex transpose operation:

$$\mathbf{K}^\dagger = (\mathbf{d}\mathbf{d}^\dagger)^\dagger = \mathbf{d}\mathbf{d}^\dagger = \mathbf{K} \tag{2.13}$$

Using these vectors and matrices, Eq. 2.12 becomes:

$$B_{Bart}(\theta_s) = \mathbf{w}^\dagger(\theta_s)\mathbf{K}(\theta_{true})\mathbf{w}(\theta_s) \equiv \mathbf{w}^\dagger\mathbf{K}\mathbf{w} \tag{2.14}$$

In this equation, θ_{true} indicates the direction from which the signal is incident. This equation again provides a plot showing the incident angle of the source.

Adaptive Beamforming

Adaptive beamforming is a method of supressing the sidelobes of a traditional beamformer. It uses the incoming signal to build the weight vectors. There are many different types of adaptive beamforming, but the one presented here is the Minimum Variance distortionless processor (MV).

First, a weight vector needs to be defined that will attenuate the beamformer's output in every direction except the signal's incident angle. The weight vector that minimizes the functional can be written as:

$$F = \mathbf{w}_{MV}^\dagger \mathbf{K}\mathbf{w}_{MV} + \gamma(\mathbf{w}_{MV}^\dagger \mathbf{w} - 1) \tag{2.15}$$

The second term in this equation utilizes a Lagrangian multiplier γ in order to include the unity gain in the look direction. Several properties and methods can be used to solve for $\mathbf{w}_{MV}$ here. First, $\mathbf{K}$ is Hermitian; that is, it is a square matrix that is equal to its own conjugate transpose. Next, because a Lagrange multiplier is being used, the gradient can be found with respect to the variable $\mathbf{w}_{MV}$ and it can be set equal to zero:

$$2\mathbf{K}\mathbf{w}_{MV} + \gamma\mathbf{w} = 0 \tag{2.16}$$

This gives:

$$\mathbf{w}_{MV} = -\frac{\gamma}{2}\mathbf{K}^{-1}\mathbf{w} \longrightarrow \mathbf{w}_{MV}^{\dagger} = -\frac{\gamma}{2}(\mathbf{K}^{-1}\mathbf{w})^{\dagger} \tag{2.17}$$

Using the second term of Eq. 2.15 as the unity gain in the look direction:

$$\frac{\partial F}{\partial \gamma} = \mathbf{w}_{MV}^{\dagger}\mathbf{w} - 1 = 0 \tag{2.18}$$

Combining these equations results in:

$$\gamma = -2(\mathbf{w}^{\dagger}\mathbf{K}^{-1}\mathbf{w})^{-1} \tag{2.19}$$

This equation can then be used to find an expression for $\mathbf{w}_{MV}$:

$$\mathbf{w}_{MV} = \frac{\mathbf{K}^{-1}\mathbf{w}}{\mathbf{w}^{\dagger}\mathbf{K}^{-1}\mathbf{w}} \tag{2.20}$$

This weight vector follows the standards of adaptive beamforming in that it utilizes the received data to construct the weight vector that is then applied to the received data. This weight vector can now be used in Eq. 2.14:

$$B_{MV}(\theta_s) = [\mathbf{w}^{\dagger}(\theta_s)\mathbf{K}^{-1}(\theta_{true})\mathbf{w}(\theta_s)]^{-1} \tag{2.21}$$

The Minimum Variance distortionless beamformer is a high-resolution beamformer. It is designed to suppress the sidelobes and have a narrower main lobe than typical plane wave beamformers. While it performs this function very well, it is most effective with correlated noise, which is not present in the cases in this paper.

Near Field Beamforming

Far field beamforming, while quite convenient and accurate in far field, free field measurements, loses its precision in near field, multipath environments where the far field assumptions cannot be made. Many different methods have been developed to simplify the near field problem. Several of these will be discussed, starting with the method chosen for this thesis.

Near Field Compensation

This method accounts for the spherical nature of wavefronts and calculates the path length difference to each element in the array. It uses the same method as the delay and sum beamforming in the frequency domain from the beginning of the chapter, but without making the far field assumptions.

Starting with Eq. 2.1, far field assumptions cannot be made, so this equation becomes:

$$p(r,\theta,t) = Ae^{j\omega t}\sum_{i=1}^{N}\frac{1}{r_i}e^{j(\phi_i - kr_i)} \tag{2.22}$$

Note that a phase delay ϕ_i has been added which, as in the far field case, can be defined as $\phi_i = ik\Delta r_i$. The solution for Δr_i for the near field case will be presented later. Again, the frequency domain is the domain of choice for this thesis, so an FFT of this equation gives

$$F(\omega) = \frac{1}{2\pi}\int_{-T/2}^{T/2} Ae^{j\omega t}\left(\sum_{i=1}^{N}\frac{1}{r_i}e^{j(\phi_i - kr_i)}\right)e^{-j\omega t}dt \tag{2.23}$$

and can be simplified to

$$F(\omega) = \frac{1}{2\pi}A\sum_{i=1}N\frac{1}{r_i}e^{j(\phi_i - kr_i)}\int_{-T/2}^{T/2}dt \tag{2.24}$$

Once again, it appears the only addition to the unsteered FFT is a phase delay term that is now dependent on both steering angle and range. To find that range, the path length difference must be recalculated for each element. By varying both slant range and look direction, the

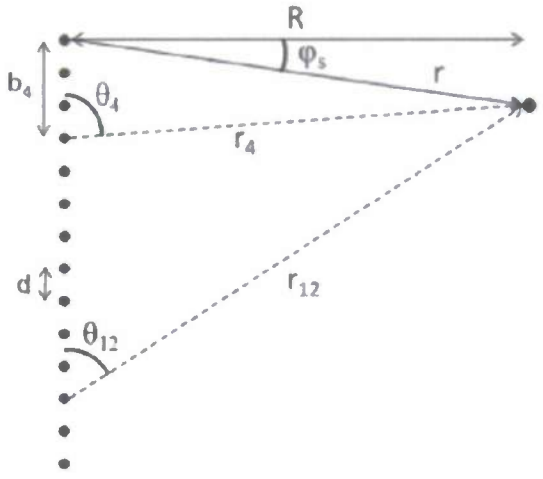

Figure 2.5: Near Field Equation Geometry

range to each element can be found using the known array geometry (Figure 2.5) and the Law of Cosines

$$r_i = \sqrt{r^2 + b_i^2 - 2rb_i \cos(90 + \varphi_s)} \tag{2.25}$$

where $b_i = (i-1)d$ and φ_s is the steering angle. Δr_i can then be computed

$$\Delta r_i = r_i - r \tag{2.26}$$

This Δr_i can be inserted into Eq. 2.10 and subsequently Eq. 2.8. This will compute a BTR for a fixed range. By varying r in Eq. 2.25, a map of possible locations of the source based on slant range and look direction is created. Figure 2.6 shows the output of this algorithm.

The location of the maximum of this plot is the location of the source and is represented by the diamond. The BTR can be examined at the peak's range if we are interested in the evolution of the signal's location over time.

This is a very simple, yet extremely flexible method of beamforming, hence the reason it is used in this paper. Some other methods are now presented to show the different algorithms for near field beamforming that have been established.

Matched-Field Processing

Matched-Field Processing (MFP) is a processing technique that adds an additional dimension to the traditional plane wave beamformer. Jensen covers the subject of MFP in [3]. In both cases, the data is matched to a replica field. In Conventional Beamforming, that replica is plane waves, where in Matched-Field Processing, the replica consists of the theoretical field using dimensions of angle and range. This allows the MFP to localize in angle and range as opposed to only detecting an incident angle, as is done in CBF. Instead of only scanning through steering angles,

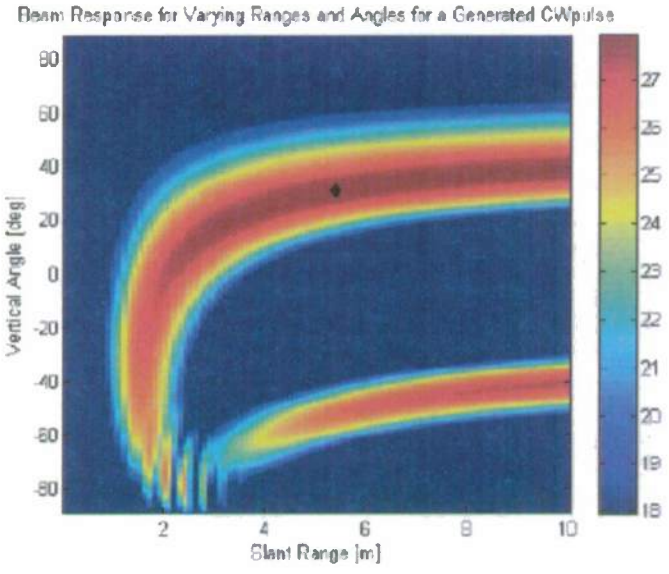

Figure 2.6: Sample Near Field Plot

a generated source is placed at various points in an angle/range search grid. The transmission path is then calculated using standard propagation models, and the theoretical result is placed into a replica matrix. This matrix is then correlated with the real data, and the true location is at the peak of the correlation.

The MFP algorithm can be modeled just like a plane wave beamformer such as in Eq. 2.14. Now, instead of constructing the weight vector, w, using a simple far field approximation method, the wave equation can be used to come up with the theoretical results for each source search location, a. $\mathbf{K}(\mathbf{a}_{true})$ represents the real data that is matched against the replica.

$$B_{Bart}(\mathbf{a}) = \mathbf{w}^{\dagger}(\mathbf{a})\mathbf{K}(\mathbf{a}_{true})\mathbf{w}(\mathbf{a}) \tag{2.27}$$

Here, the max of $B_{Bart}(\mathbf{a})$ is at the real source location, $\mathbf{a}_{true}$. As in the CBF case, the MFP possesses sidelobes that are present in the form of "ambiguous peaks." These peaks can be suppressed by adaptive algorithms, such as the Minimum Variance processor, by adding the range dimension to the algorithm.

$$B_{MV}(\mathbf{a}) = [\mathbf{w}^{\dagger}(\mathbf{a})\mathbf{K}^{-1}(\mathbf{a}_{true})\mathbf{w}(\mathbf{a})]^{-1} \tag{2.28}$$

Once again, the real source location, $\mathbf{a}_{true}$, is located at the max of $B_{MV}(\mathbf{a})$.

This only scratches the surface of the realm of MFP, but [3] has a list of various applications and references for many of the algorithms that have been developed.

Radial Reciprocity

One method of near field beamforming that was developed by [1, 2] uses a near field-far field radial beampattern transformation. This method takes a near field beampattern and converts it to an equivalent far field beampattern for a specific frequency, but this can be expanded to broadband usage.

They start with a beampattern $b \equiv b(r, \theta, \phi, t)$ as a solution to the wave equation expressed in spherical coordinates:

$$\frac{1}{r^2}\frac{\partial}{\partial r}\left(r^2\frac{\partial b}{\partial r}\right) + \frac{1}{r^2\sin\theta}\frac{\partial}{\partial\theta}\left(\sin\theta\frac{\partial b}{\partial\theta}\right) + \frac{1}{r^2\sin^2\theta}\frac{\partial^2 b}{\partial\phi^2} = \frac{1}{c^2}\frac{\partial^2 b}{\partial t^2} \tag{2.29}$$

The solution is then presented as:

$$b_r(\theta,\phi;k) = r^{-(1/2)}\left(\sum_{n=0}^{\infty}\alpha_n H^{(1)}_{n+1/2}(kr)P_n(\cos\theta) + \ldots \right.$$
$$\left. \ldots \sum_{n=1}^{\infty}\sum_{m=1}^{\infty} H^{(1)}_{n+1/2}(kr)P_n^m(\cos\theta)\times(\beta_{nm}e^{jm\phi} + \gamma_{nm}e^{-jm\phi})\right) \tag{2.30}$$

where $k = \frac{2\pi f}{c}$ is the wavenumber, $P_n(\cdot)$ is the nth order Legendre function, $P_n^m(\cdot)$ are the associated Legendre functions, and the half integer order Hankel function of the first kind is written as:

$$H^{(1)}_{n+1/2}(\cdot) = J_{n+1/2}(\cdot) + jY_{n+1/2}(\cdot)$$

where $J_{n+1/2}(\cdot)$ is a half integer order Bessel function of the first kind, and $Y_{n+1/2}(\cdot)$ is a half integer order Neumann function (also a Bessel function of the second kind).

The coefficients α_n, β_{nm}, and γ_{nm} can be defined as:

$$\alpha_n = \frac{n+\frac{1}{2}}{2\pi r^{-(1/2)}H^{(1)}_{n+1/2}(kr)} \times \int_0^{2\pi}\int_0^{\pi} b_r(\theta,\phi;k)P_n(\cos\theta)\sin\theta\, d\theta\, d\phi \tag{2.31}$$

$$\beta_{nm} = \frac{n+\frac{1}{2}}{2\pi r^{-(1/2)}H^{(1)}_{n+1/2}(kr)}\frac{(n-m)!}{(n+m)!} \times \int_0^{2\pi}\int_0^{\pi} b_r(\theta,\phi;k)P_n^m(\cos\theta)\sin\theta e^{-jm\phi}\, d\theta\, d\phi \tag{2.32}$$

$$\gamma_{nm} = \frac{n+\frac{1}{2}}{2\pi r^{-(1/2)}H^{(1)}_{n+1/2}(kr)}\frac{(n-m)!}{(n+m)!} \times \int_0^{2\pi}\int_0^{\pi} b_r(\theta,\phi;k)P_n^m(\cos\theta)\sin\theta e^{jm\phi}\, d\theta\, d\phi \tag{2.33}$$

Because the coefficients in Eq. 2.30 fully describe the beam pattern at any range, it can be rewritten for sources at any point in space, allowing a near field beampattern to be transformed to a far field beampattern, moving from a finite sphere in the near field to an infinite sphere in the far field.

The following steps outline the procedure of using this transformation.

1) Find α_n, β_{nm}, and γ_{nm} for the wanted nearfield beampattern $b_{r_d}(\theta,\phi;k)$ where $r = r_d$.

2) Use Eq. 2.30 to calculate $b_\infty(\theta,\phi;k)$ at $r = \infty$.

3) Design a farfield beamformer to create this desired beampattern.

The far field synthesis equation is established in [1]:

$$\tilde{b}_{\infty}(\theta, \phi; k) \sim \sqrt{\frac{2}{\pi k}} e^{j(k-k_0)} \left(\sum_{n=0}^{\infty} \alpha_n (-j)^{n+1} P_n(\cos\theta) + \dots \right) \tag{2.34}$$

A special case for linear arrays is also explored. This reduces Eqs. 2.30 and 2.31 coefficients to two very simple equations:

$$b_r(\theta; k) = \sum_{n=0}^{\infty} \alpha_n r^{-1/2} H^{(1)}_{n+1/2}(kr) P_n(\cos\theta) \tag{2.35}$$

$$\alpha_n = \frac{n+\frac{1}{2}}{r^{-1/2} H^{(1)}_{n+1/2}(kr)} \int_0^{\pi} b_r(\theta; k) P_n(\cos\theta) \sin\theta \, d\theta \tag{2.36}$$

This results in a much simpler synthesis equation:

$$\tilde{b}_{\infty}(\theta; k) \sim \sqrt{\frac{2}{\pi k}} e^{j(k-k_0)} \sum_{n=0}^{\infty} \alpha_n (-j)^{n+1} P_n(\cos\theta) \tag{2.37}$$

This gives a simplified method of creating a radial beampattern near field-far field transformation for a specific case. Further details can be found in [1, 2].

Robust Near-Field Adaptive Beamforming

Near field adaptive beamforming was explored by Zheng, Goubran, and El-Tanany in [4]. They tackle the robustness problem of creating an adaptive beamformer for the near field. They go on to cite the advantage of distance discrimintation using their algorithm, saying "The proposed beamformer can simultaneously improve the distance discrimination and the robustness against location errors without additional constraints."

Zheng starts by defining a beamformer with elements located at $\mathbf{x}_m = (r_m, \theta_m, \phi_m)$ in the spherical coordinate system, as shown in Figure 2.7, where $m = 1, 2, \dots, M$ and where M is the number of elements in the array. Note that the meanings of θ and ϕ represent the azimuthal angle and polar angle respectively. These definitions are common in mathematics, however they are opposite the typical convention found in physics. This has no bearing on the equations in this section. They also define K as the number of taps. Assume the source is located at $\mathbf{x}_s = (r_s, \theta_s, \phi_s)$ and that it is within our near field parameters as defined in Eq. 1.1. The near field steering vector would need to be used

$$\mathbf{a}(\mathbf{x}_s, f) = \frac{r_s}{e^{j2\pi f r_s/c}} \left[\frac{e^{j2\pi f r_{1s}/c}}{r_{1s}}, \dots, \frac{e^{j2\pi f (r_{ms}/c - k)}}{r_{ms}}, \dots, \frac{e^{j2\pi f (r_{Ms}/c - K+1)}}{r_{Ms}} \right]^T \tag{2.38}$$

where T indicates the transpose operation, f is the operating frequency, c is the sound speed,

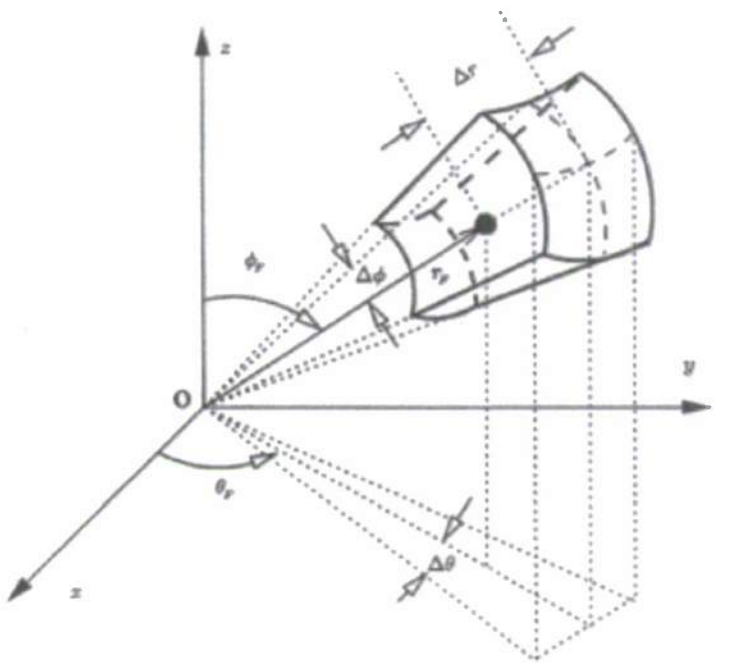

Figure 2.7: Constrained spatial region $\Omega = (\pm\Delta r, \pm\Delta\theta, \pm\Delta\phi)$. The presumed focal point is $\mathbf{x}_F = (r_F, \theta_F, \phi_F)$. (Figure taken from [4])

$r_s = |\mathbf{x}_s|$ is the absolute distance from the source to the center of the array, and $r_{ms} = |\mathbf{x}_m - \mathbf{x}_s|$ is the absolute distance from the source to the mth element of the array. If the input to the beamformer is allowed to be samples in a vector $N = MK$ and define it as $\mathbf{u}(k)$, where k is the tap index. The output of the beamformer can be defined simply as $y(k) = \mathbf{w}^H\mathbf{u}(k)$, where $\mathbf{w}$ is the weight vector and H is the complex conjugate transpose operation. The linearly constrained minimum variance (LCMV) beamforming method can then be used to minimize the output power around constraints

$$\min_{\mathbf{w}} [\mathbf{w}^H\mathbf{R}_{\mathbf{uu}}\mathbf{w}] \tag{2.39}$$

$$\text{subject to } \mathbf{C}^H\mathbf{w} = \mathbf{h} \tag{2.40}$$

where $\mathbf{R}_{\mathbf{uu}}$ is the NxN covariance matrix of the input vector, $\mathbf{u}$. In this case, $\mathbf{h}$ is the wanted response vector and $\mathbf{C}$ is the matrix of constraints. This gives an optimal solution

$$\mathbf{w}_{opt} = \mathbf{R}_{\mathbf{uu}}{}^{-1}\mathbf{C}(\mathbf{C}^H\mathbf{R}_{\mathbf{uu}}{}^{-1}\mathbf{C})^{-1}\mathbf{h} \tag{2.41}$$

which can be broken into two components

$$\mathbf{w}_q = \mathbf{C}(\mathbf{C}^H\mathbf{C})^{-1}\mathbf{h} \tag{2.42}$$

$$\mathbf{w}_a = (\mathbf{C}_a^H\mathbf{R}_{\mathbf{uu}}\mathbf{C}_a)^{-1}\mathbf{C}_a^H\mathbf{R}_{\mathbf{uu}}\mathbf{w}_q \tag{2.43}$$

where $\mathbf{w}_q$ is the fixed beamformer component, $\mathbf{w}_a$ is the unconstrained adaptive component, and $\mathbf{C}_a$ is the signal blocking matrix. The solution to $\mathbf{w}_a$ using the normalized least mean square (NLMS) algorithm can be written

$$\mathbf{w}_a(k+1) = \mathbf{w}_a(k) + \mu\frac{\mathbf{u}(k)e(k)}{\mathbf{u}^H(k)\mathbf{u}(k)} \tag{2.44}$$

where the error is $e(k) = [\mathbf{w}_q - \mathbf{C}_a\mathbf{w}_a]^H\mathbf{u}(k)$ and the step size is μ. The robustness issue can now be explored. Consider a signal in a region $\Omega = (\pm\Delta r, \pm\Delta\theta, \pm\Delta\phi)$ around a focal point $\mathbf{x}_F = (r_F, \theta_F, \phi_F)$, and a frequency band B. If the source sample vector is defined as $\mathbf{s}(k)$ and the power spectrum density as $S(f)$, then the covariance matrix can be written as

$$\mathbf{R}_{\mathbf{ss}} = E\{\mathbf{s}(k)\mathbf{s}^T(k)\} = \frac{1}{\Omega}\frac{1}{B}\int_{\Omega}\int_{B} S(f)\mathbf{a}(\mathbf{x}, f)\mathbf{a}^H(\mathbf{x}, f)df d\mathbf{x} \tag{2.45}$$

where $\mathbf{a}(\mathbf{x}, f)$ is defined in Eq. 2.38. A Karhunen-Loeve expansion can be performed on the sample vector $\mathbf{s}(k)$ and becomes $\mathbf{s}(k) = \sum_{n=1}^{N} s_n\mathbf{v}_n$ where $s_n = \mathbf{v}_n^T\mathbf{s}(k)$. Approximating this expansion gives

$$\mathbf{s}(k) \approx \hat{\mathbf{s}}(k) = \sum_{n=1}^{L} s_n\mathbf{v}_n \tag{2.46}$$

The eigenvalues λ_n correspond to the energy of the sample vector projected onto $\mathbf{v}_n$. L is chosen to obtain an approximation error that can be written as

$$\epsilon(L) = E\{|\mathbf{s}(k) - \hat{\mathbf{s}}(k)|^2\} = \sum_{n=L+1}^{N} \mathbf{v}_n^T\mathbf{R}_{\mathbf{ss}}\mathbf{v}_n = \sum_{n=L+1}^{N} \lambda_n \tag{2.47}$$

The eigenvalues of a broadband signal decrease quickly when $n < \beta$, where $\beta = 2BT(\mathbf{x}_s)$, and $T(\mathbf{x}_s)$ is the length of the time window as a function of the source location

$$T(\mathbf{x}_s) = \tau(\mathbf{x}_s) + K - 1 \tag{2.48}$$

where $\tau(\mathbf{x}_s) = [\max(r_{ms}) - \min(r_{ms})]/c/F_s$ where F_s is the sampling frequency. The constraint design method can now be established. If a flat spectrum in B is assumed, $\mathbf{R}_{\mathbf{ss}}$ can be easily solved for

$$\mathbf{R}_{\mathbf{ss}} = \frac{1}{P}\sum_{i=1}^{I}\sum_{j=1}^{J}\mathbf{a}(\mathbf{x}_i, f_j)\mathbf{a}^H(\mathbf{x}_i, f_j) = \frac{1}{P}\mathbf{A}\mathbf{A}^T \tag{2.49}$$

where $P = IJ$ and $\mathbf{A}$ is defined as

$$\mathbf{A} = [\mathbf{a}_c(\mathbf{x}_1, f_1), \ldots, \mathbf{a}_c(\mathbf{x}_i, f_j), \ldots, \mathbf{a}_c(\mathbf{x}_I, f_J) | \mathbf{a}_s(\mathbf{x}_1, f_1), \ldots, \mathbf{a}_s(\mathbf{x}_i, f_j), \ldots, \mathbf{a}_s(\mathbf{x}_I, f_J)] \quad (2.50)$$

where $\mathbf{a}_c(\mathbf{x}_i, f_j)$ and $\mathbf{a}_s(\mathbf{x}_i, f_j)$ are the real and imaginary parts of the steering vector. Meanwhile the constraint equation can be written as

$$\mathbf{A}^T \mathbf{w} = \mathbf{g} \quad (2.51)$$

where $\mathbf{g}$ is the response vector

$$\mathbf{g} = [g_{11} \cos(2\pi f_1 \tau_1), \ldots, g_{IJ} \cos(2\pi f_J \tau_I) | g_{11} \sin(2\pi f_1 \tau_1), \ldots, g_{IJ} \sin(2\pi f_J \tau_I)]^T \quad (2.52)$$

τ_i is the group delay of the signal at location $\mathbf{x}_i$ relative to the origin and g_{ij} are the desired amplitude responses. The singular value decomposition (SVD) of $\mathbf{A}$ can be used to find the low rank representation of $\mathbf{R}_{ss}$

$$\mathbf{A} = \mathbf{V}\boldsymbol{\Sigma}\mathbf{U}^T \quad (2.53)$$

where $\boldsymbol{\Sigma}$ is a diagonal matrix of the values $\sigma_1, \sigma_2, \ldots, \sigma_N$ of $\mathbf{A}$ in a descending order and the columns of $\mathbf{V}$ and $\mathbf{U}$ are the singular vectors. The values of $\mathbf{A}$ are related by $\lambda_n = \sigma_n^2/P$ to the eigenvalues of $\mathbf{R}_{ss}$. Therefore,

$$\mathbf{A} \approx \mathbf{A}_L = \mathbf{V}_L \boldsymbol{\Sigma}_L \mathbf{U}_L^T \quad (2.54)$$

where the columns of $\mathbf{V}_L$ and $\mathbf{U}_L$ are the L columns of $\mathbf{V}$ and $\mathbf{U}$ for the L singular values and $\boldsymbol{\Sigma}_L = \text{diag}\{\sigma_1, \sigma_2, \ldots, \sigma_L\}$. Combining Eqs. 2.51 and 2.54 gives $\mathbf{V}_L^T \mathbf{w} = \boldsymbol{\Sigma}_L^{-1} \mathbf{U}_L^T \mathbf{g}$ which allows a constraint equation to be designed

$$\begin{aligned} \mathbf{C} &= \mathbf{V}_L \\ \mathbf{h} &= \boldsymbol{\Sigma}_L^{-1} \mathbf{U}_L^T \mathbf{g} \end{aligned} \quad (2.55)$$

The procedures to design this beamformer are summarized by [4] as follows:

1) Select a large number of points I and J in a specified constraint region Ω and frequency band B, respectively; Form the matrix $\mathbf{A}$ as in 2.50 and the desired response vector $\mathbf{g}$ as in 2.52;

2) Perform the singular value decomposition (SVD) of $\mathbf{A}$. Find the matrices $\mathbf{V}$, $\boldsymbol{\Sigma}$, and $\mathbf{U}$ as in 2.53.

3) Specify an approximation error $\epsilon(L)$. For example, an error level of -40 dB is sufficient for unit gain constraints. Then find the required number of constraints L by computing the approximation error as in 2.47;

4) Form Σ_L, $\mathbf{V}_L$, and $\mathbf{U}_L$ by choosing the largest L singular values in Σ and the corresponding L column vectors in $\mathbf{V}$ and $\mathbf{U}$, respectively;

5) Compute the linear constraints $\mathbf{C}$ and $\mathbf{h}$ as in 2.55;

6) To implement the adaptive beamformer in the GSC structure, compute $\mathbf{w}_q$ as in 2.43 and $\mathbf{w}_a$ as in 2.43 or 2.44.

This method of near field beamforming is based on the far field LCMV beamforming algorithm. While this seems to be an effective method of near field beamforming, the LCMV beamformer with Zheng's robustness algorithm is not the method chosen for this thesis.

Chirp Zeta Transform

Another method of near field 3-D imaging exploits the computational ease of the Chirp Zeta transform (CZT) algorithm and was presented in [5] and [6]. A two dimensional array must be used, as scanning in three dimensional space requires two different steering angles. Thus, a planar array composed of M x N elements is used. The previously defined d is the separation distance between elements. Following time-domain beamforming convention for two steering directions, the beam signal can be written as

$$b(t, \theta_{ap}, \theta_{eq}) = \sum_{m=0}^{M-1} \sum_{n=0}^{N-1} w_{m,n} s_{m,n}(t - \tau(r_0, \theta_{ap}, \theta_{eq}, m, n)) \tag{2.56}$$

for $0 \leq p \leq M_b - 1$ and $0 \leq q \leq N_b - 1$ where p and q are the beam signal indexes and subscripts a and e refer to the azimuth and elevation directions. Also, the time delay, τ, can be expressed as

$$\tau(r_0, \theta_{ap}, \theta_{eq}, m, n) = \frac{r_0 - \sqrt{x}}{c} \tag{2.57}$$

where

$$x = r_0^2 + ((m - M/2)d)^2 + ((n - N/2)d)^2 - 2(m - M/2)r_0 d \sin\theta_{ap} - 2(n - N/2)r_0 d \sin\theta_{eq}$$

and $s_{m,n}(t)$ is the incoming signal, while $w_{m,n}$ is the weight factor that controls the sidelobe levels. As usual, c is the sound speed. If the Fresnel approximation is assumed, τ becomes

$$\tau(r_0, \theta_{ap}, \theta_{eq}, m, n) = \frac{(m - M/2)d \sin\theta_{ap}}{c} + \cdots$$
$$\cdots \frac{(n - N/2)d \sin\theta_{eq}}{c} - \frac{((m - M/2)d)^2 - ((n - N/2)d)^2}{2r_0 c} \tag{2.58}$$

The signal is then broken into snapshots of length K and converted into the frequency domain. This results in the beam signal $b(t, \theta_{ap}, \theta_{eq})$ becoming

$$B(k,\theta_{ap},\theta_{eq}) = \sum_{m=0}^{M-1}\sum_{n=0}^{N-1} w_{m,n}S_{m,n}(k)\cdot\exp\left(-j2\pi f_k\left(\frac{md\sin\theta_{ap}}{c}+\frac{nd\sin\theta_{eq}}{c}\right)\right)\cdot$$
$$\cdot\exp(j2\pi f_k\gamma(m,n,p,q)) \tag{2.59}$$

where

$$\gamma(m,n,p,q) = \frac{(M/2)d\sin\theta_{ap}}{c}+\frac{(N/2)d\sin\theta_{eq}}{c}+\frac{((m-M/2)d)^2}{2r_0c}+\frac{((n-N/2)d)^2}{2r_0c} \tag{2.60}$$

Note that in Eq. 2.60, the first two terms are dependent on steering angles, but not on the indexes. For now these terms can be thrown out and revisited later. This now gives a simplified form of Eq. 2.60

$$\gamma(m,n) = \frac{((m-M/2)d)^2}{2r_0c}+\frac{((n-N/2)d)^2}{2r_0c} \tag{2.61}$$

Eq. 2.59 can be further simplified by defining

$$z_{\theta_{ap}}z_{\theta_{eq}} = \exp\left(-j2\pi f_k\frac{d\sin\theta_{ap}}{c}\right)\exp\left(-j2\pi f_k\frac{d\sin\theta_{eq}}{c}\right) \tag{2.62}$$

$$v_{m,n} = w_{m,n}\exp(j2\pi f_k\gamma_{m,n}) \tag{2.63}$$

and rewriting it as

$$B(k,\theta_{ap},\theta_{eq}) = \sum_{m=0}^{M-1}\sum_{n=0}^{N-1} v_{m,n}S_{m,n}(k)z_{\theta_{ap}}^{n}z_{\theta_{eq}}^{m} \tag{2.64}$$

If k is held constant, the CZT algorithm can be utilized. This allows a series of variables to be set relating to the azimuth and elevation angles:

$$A_a = \exp\left(-j2\pi f_k\frac{d}{c}\sin\theta_{ai}\right)$$
$$W_a = \exp\left(j2\pi f_k\frac{d}{c}\Delta s_a\right) \tag{2.65}$$
$$\Delta s_a = \frac{\sin\theta_{af}-\sin\theta_{ai}}{M_b-1}$$

and

$$A_e = \exp\left(-j2\pi f_k\frac{d}{c}\sin\theta_{ei}\right)$$

$$W_c = \exp\left(j2\pi f_k \frac{d}{c}\Delta s_c\right) \tag{2.66}$$
$$\Delta s_c = \frac{\sin\theta_{cf} - \sin\theta_{ci}}{M_b - 1}$$

where the i and f additions to the subscripts indicate the initial and final steering angles. These angles can be used to find the angles θ_{ap} and θ_{cq}

$$\sin\theta_{ap} = \sin\theta_{ai} + \Delta s_a p \qquad p = 0, \ldots, M_b - 1 \tag{2.67}$$
$$\sin\theta_{cq} = \sin\theta_{ci} + \Delta s_c q \qquad q = 0, \ldots, N_b - 1 \tag{2.68}$$

Finally, Eq. 2.59 can be written in a form using the CZT algorithm

$$B(k, \theta_{ap}, \theta_{cq}) = W_a^{\frac{-p^2}{2}} W_c^{\frac{-q^2}{2}} \sum_{m=0}^{M-1} \sum_{n=0}^{N-1} v_{m,n} S_{m,n}(k) A_a^m A_c^n W_a^{\frac{-m^2}{2}} W_c^{\frac{-n^2}{2}} W_a^{\frac{(p-m)^2}{2}} W_c^{\frac{(q-n)^2}{2}} \tag{2.69}$$

This equation can be represented by a convolution of two matrices

$$\mathrm{C}(k) = v_{m,n} S_{m,n}(k) A_a^m A_c^n W_a^{\frac{-m^2}{2}} W_c^{\frac{-n^2}{2}} \tag{2.70}$$
$$\mathrm{D} = W_a^{\frac{m^2}{2}} W_c^{\frac{n^2}{2}}$$

This allows for fast computing using convolution methods. After all the beams are calculated, an inverse Fourier Transform will reveal the beam signal.

This method is effective and is a computationally easy load. However, this study involves data collected using a 1-D array, and this algorithm is designed for a planar array. This, therefore, is not the method that was chosen for this work.

Many different post-processing methods were presented in this chapter. Of the methods presented, the ones chosen for this work were the basic frequency domain, far field beamforming and the near field compensation method of near field beamforming. These will be used in Chapter 4 to analyze the data that was collected. The next chapter will describe the instrumentation used and the geometries of the test layouts.

IMPACT

This study examined data acquired at the Navy's Acoustic Research Detachment at Lake Pend Oreille in Bayview, Idaho and processed the data using a near field compensation beamforming algorithm with a modification to account for array curvature. The improvements in the accuracy of this modification were presented as well.

Several methods of both far field and near field beamforming were presented, including the methods used. Each method has its benefits as well as its disadvantages, and the simplest method with the ability to adjust to a non-linear array was chosen.

The array and test site geometry, as well as the various equipment that was used in testing, was briefly discussed. The many signals that were transmitted were also presented.

Results of the processed data were presented. Results were first presented for the case of an array in deep water with the source in the far field. A method of far field beamforming was used to determine the location of the source, followed by results of using the near field compensation method of beamforming to be sure the near field algorithm worked properly while the source was in the far field. The array was then moved into the near field of the source and it was proven that a far field beamforming method would not work. The near field algorithm was then used, accompanied by a method for accounting for a non-linear array, followed by a discussion of the accuracy of this modification. The array and source were then moved into shallow water where many reflections were present. The near field algorithm with the array curvature modification was used to analyze a CW pulse, a LFM pulse, and broadband noise. The results presented showed that this method improved the accuracy of the near field compensation beamformer for all cases of a CW pulse and LFM pulse. Broadband noise was less accurate, however it was postulated that this was due to movement of the array during the course of the data collection event.

RELATED PROJECTS (N/A)

REFERENCES

[1] KENNEDY, R. A., T. D. ABHAYAPALA, and D. B. WARD (1998) "Broadband Nearfield Beamforming Using a Radial Beampattern Transformation," *IEEE Transactions on Signal Processing*, 46(8), pp. 2147–2156.

[2] KENNEDY, R. A., D. B. WARD, and T. D. ABHAYAPALA (1999) "Nearfield Beamforming Using Radial Reciprocity," *IEEE Transactions on Signal Processing*, 47(1), pp. 33–40.

[3] JENSEN, F. B., W. A. KUPERMAN, M. B. PORTER, and H. SCHMIDT (2000) *Computational Ocean Acoustics*, Springer-Verlag.

[4] ZHENG, Y. R., R. A. GOUBRAN, and M. EL-TANANY (2004) "Robust Near-Field Adaptive Beamforming With Distance Discrimination," *IEEE Transactions on Speech and Audio Processing*, 12(5), pp. 478–488.

[5] PALMESE, M., G. DE TONI, and A. TRUCCO (2006) "3-D Underwater Acoustic Imaging by an Efficient Frequency Domain Beamforming," in *Proceedings of the 2006 IEEE International Workshop on Imaging Systems and Techniques - IST 2006*, pp. 86–90.

[6] PALMESE, M. and A. TRUCCO (2007) "Digital Near Field Beamforming for Efficient 3-D Underwater Acoustic Image Generation," in *IEEE International Workshop on Imaging Systems and Techniques - IST 2007*, pp. 1–5.

[7] BURDIC, W. S. (1991) *Underwater Acoustic System Analysis*, Prentice Hall.

[8] KINSLER, L. E., A. R. FREY, A. B. COPPENS, and J. V. SANDERS (2000) *Fundamentals of Acoustics: Fourth Edition*, John Wiley and Sons, Inc.

[9] MARANDA, B. (1989) "Efficient digital beamforming in the frequency domain," *Journal of the Acoustical Society of America*, 86(5), pp. 1813–1819.

[10] ABRAHAM, D. (2010) "Array Signal Processing for Sonar: Short Course," in *159th Meeting of the Acoustical Society of America*.

PUBLICATIONS (N/A)

HONORS/AWARDS/PRIZES

Brian E. Fowler received his Masters of Engineering, May 2013.